National Conference with International Participation

ENGINEERING MECHANICS 2008

Svratka, Czech Republic, May 12 – 15, 2008

MICROSTRUCTURE-BASED MODELING OF ELASTIC FUNCTIONALLY GRADED MATERIALS

Z. Sharif Khodaei*, J. Zeman **

Summary: *Functionally graded materials (FGMs) are two-phase composites with continuously changing microstructure adapted to performance requirements. Traditionally, the overall behavior of FGMs has been determined using local averaging techniques or a given smooth variation of material properties. Although these models are computationally efficient, their validity and accuracy remain questionable as a link with the underlying microstructure (including its randomness) is not clear. In this paper, we propose a modeling strategy for the linear elastic analysis of FGMs systematically based on a realistic microstructural model. The overall response of FGMs is addressed in the framework of stochastic Hashin-Shtrikman variational principles. To allow for the analysis of finite bodies, recently introduced discretization schemes based on the Finite Element Method and the Boundary Element Method are employed to obtain statistics of local fields. Representative numerical examples are presented to compare the performance and accuracy of both schemes. To gain insight into similarities and differences between these methods and to minimize technicalities, the analysis is performed in the one-dimensional setting.*

1. Introduction

As typical of all composites, the analysis of functionally graded materials is complicated by the fact that the explicit discrete modeling of the material microstructure results in a problem which is intractable due to huge number degrees of freedom and/or its intrinsic randomness. As the most straightforward answer to this obstacle, models with a given smoothly varying material data are often employed. When the spatial non-homogeneity is assumed to follow a sufficiently simple form, this premise opens the route to very efficient numerical schemes, such as specialized finite elements (Santare and Lambros, 2000), boundary element techniques (Sutradhar and Paulino, 2004) or local integral equations (Sládek et al., 2005).

Thanks to their simplicity, these methods can be rather easily generalized to more complex issues such as coupled thermal-mechanical problems (Noda, 1999) or crack

* Ing. Zahra Sharif Khodaei.:Czech Technical University in Prague, Faculty of Civil Engineering; Thakurova 7, 166 29 Prague 6; Tel:+420-2-24354482, Fax:+420-2-24310775, e-mail: zahra.sharif@gmail.com

** Ing. Jan Zeman, Ph.D.:Czech Technical University in Prague, Faculty of Civil Engineering; Thakurova 7, 166 29 Prague 6; Tel:+420-2-24354482, Fax:+420-2-24310775, e-mail: zemanj@cml.fsv.cvut.cz

propagation (Sekhar et al., 2005). Although this approach is very appealing from the computational point of view, its validity remains rather questionable as it contains no direct link with the underlying heterogeneous microstructure.

One possibility of establishing such a connection is to assert that the FGM locally behaves as a homogeneous composite characterized by a given volume fraction and use well-established local effective media theories. Local averaging techniques have acquired a considerable attention due to their simplicity comparable with the previous class of models. An exemplar illustration of capabilities of this modeling paradigm is the work by Goupee and Vel, (2006) which provides an efficient algorithm for FGMs composition optimization when taking into account coupled thermo-mechanical effects. Still, despite of substantial improvement in physical relevance of the model, local averaging methods may lead to inaccurate results. This was demonstrated by a systematic study of Reiter et al., (1997) and Reiter and Dvorak, (1998), which clearly show that the local averaging technique needs to be adapted to detailed character of the microstructure in a neighborhood of the analyzed material point. When considering the local averaging techniques, however, such information is evidently not available as all the microstructural data has been lumped to volume fractions only.

Another appealing approach to FGM modeling is an adaptive discrete modeling of the structure. In order to avoid the fully detailed problem, a simplified model based on, e.g., local averaging techniques, is solved first. Then, in regions where the influence of the discreteness of the microstructure is most pronounced, the microstructure with all details is recovered to obtain an accurate solution. Such a modeling strategy has been, e.g., adopted in Grujicic and Zhang, (1998) when using the Voronoi cell finite element method introduced by Ghosh et al., (1995) or recently in Vemaganti and Deshmukh, (2006) in the framework of goal-oriented modeling. Without a doubt, this approach yields the most accurate results for a given distribution of phases. However, its extension to include inevitable randomness of the microstructure seems to be an open problem.

The systematic treatment of FGMs as a random, statistically non-homogeneous composites offers, on the other hand, a possibility to apply the machinery of statistical continuum mechanics (Beran, 1968, Torquato, 2001). In this framework, overall response of the media is interpreted using the ensemble, rather than spatial, averages of the involved fields. The first class of methods stems from the description of the material composition by a non-stationary random field. This approach was pioneered by Ferrante and Graham-Brady, (2005) and further refined in Rahman and Chakraborty, (2007), where the random field description was applied to the volume fractions of the involved phases and the overall statistics was obtained using the local averaging methods. Such a strategy, however, inevitably leads to the same difficulties as in the case of deterministic analysis with a given variation of volume fractions. Alternative methods exploit the tools of mechanics of heterogeneous media. This gives rise to a correct treatment of non-local effects when combined with appropriate techniques for estimating statistics of local fields. Examples of FGMs-oriented studies include the work of Buryachenko and Rammerstorfer, (2001) who employ the multi-particle effective field method to define effective thermoelastic properties and the study by Luciano and Willis, (2004) based on the Hashin-Shtrikman energy principles; see also Buryachenko, (2001) for a comprehensive list of references in this field. Both these studies, however, work with geometrically simple domains and neglect the finite size of the microstructure.

The goal of this paper is to make the first step in formulating a model which is free of the above discussed limitations. The model itself is systematically derived from a fully penetrable sphere microstructural model introduced by Quintanilla and Torquato, (1997), which is

briefly reviewed in Section 2. The statistics of local fields then follow from re-formulation of the Hashin-Shtrikman (H-S) variational principles introduced, e.g., in Willis, 1977,Willis, (1981) and summarized in the current context in Section 3 together with the Galerkin scheme allowing to treat general bodies. Section 4 covers the application of the Finite Element Method (FEM) following Luciano and Willis, (2005, 2006) and the Boundary Element Method (BEM) in the spirit of Procházka and Šejnoha, (1996, 2003). Finally, based on results of a parametric study executed in Section 5, the comparison of both numerical scheme when applied to FGMs modeling is performed in Section 6 together with a discussion of future improvements of the model. In order to make the presentation self-contained and to minimize technicalities, the attention is restricted to a one-dimensional elasticity problem.

In the following text, we adopt the matrix notation commonly used in the finite element literature. Hence, a, $\boldsymbol{a}$ and $\mathbf{A}$ denote a scalar quantity, a vector (column matrix) and a general matrix, respectively. Other symbols and abbreviations are introduced in the text as needed.

2. Microstructural model

As already indicated in the introductory part, the morphological description adopted in this work is the one-dimensional case of a microstructural model studied in Quintanilla and Torquato, (1997). A particular realization can be depicted as a collection on N rods of length l distributed within a structure of length L, see Figure 2. The position of the i-th rod is specified by the x coordinate of its *reference point* x_i, which in our case coincides with the midpoint of a rod.

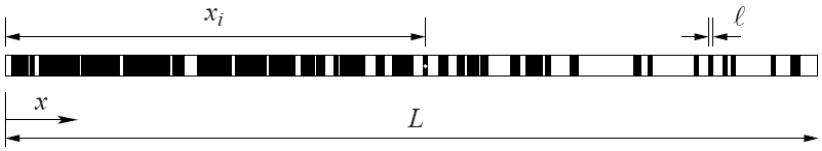

Fig. 1: Example of microstructural model realization.

The microstructure gradation is prescribed by an *intensity function* $\rho(x)$ with the product $\rho(x)\mathrm{d}x$ giving the expected number of reference points in an infinitesimal neighborhood around x. Using the theory of general Poisson processes, the probability of finding exactly m points located in a finite-sized interval I is given by Quintanilla and Torquato, (1997)

$$P_m(I) = \frac{|I|^m}{m!} \exp\left(-\int_I \rho(x)\, \mathrm{d}x\right), \tag{1}$$

where $|I|$ denotes the length of an interval I Further, to provide a suitable framework for the description of microstructure related to the model, we attach a symbol α to a particular microstructure realization (e.g., Fig 2) from a sample space $\mathbb{S}$ endowed with a probability measure p.

For a given configuration α, the distribution of a phase r is described by the characteristic function $\chi_r(x;\alpha)$

$$\chi_r(x;\alpha) = \begin{cases} 1 & \text{if } x \text{ is located in phase } r, \\ 0 & \text{otherwise,} \end{cases} \tag{2}$$

where $r = 1$ is reserved for the white phase (matrix) while $r = 2$ denotes the black phase (rod). The elementary statistical characterization of the model is provided by the *one-point probability function Sr* and the two-point probability function S_{rs}.

Finally, to provide a concrete example, consider a piecewise linear intensity function

$$\rho(x) = \begin{cases} \rho_a & 0 \le x \le a \\ \rho_a + k_\rho (x-a) & a < x \le b \\ \rho_b & b < x \le L \\ 0 & \text{otherwise} \end{cases}, \tag{3}$$

The shape of one-point probability function directly follows from the intensity profile (up to some boundary and smoothing phenomena with lengthscale l demonstrating the "geometrical" size effect present in the model). The two-point probability function then contains further details of the distribution of individual constituents.

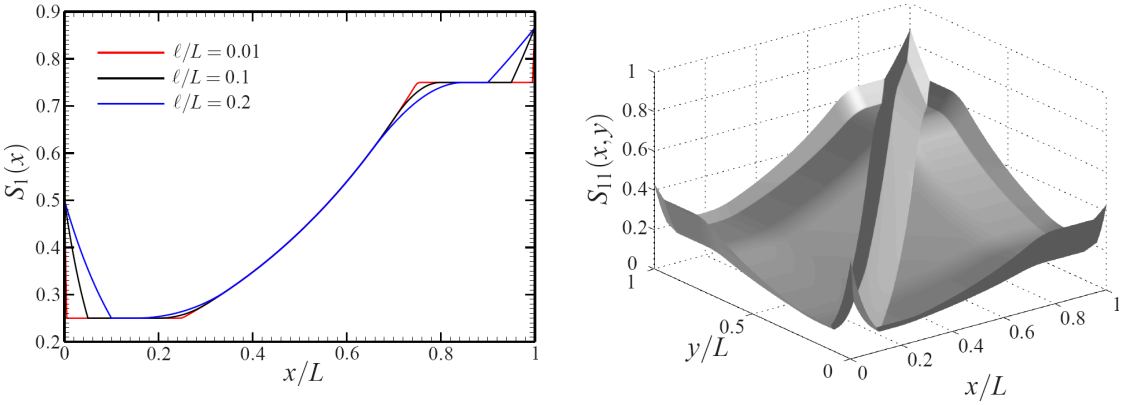

(a) (b)

Fig. 2: Examples of one- and two-point probability functions for $a = 0.25L$, $b = 0.75L$, $L = 1$ m, $\rho_a = -\log(0.25/l)$ and $\rho_b = -\log(0.75/l)$. (b) $l = 0.1$.

3. Hashin-Shtrikman variational principles

The introduced geometrical description certainly provides a solid basis for the formulation of a stochastic model of one-dimensional binary functionally graded bodies. In the sequel, we concentrate on the simplest case of linear elasticity with deterministic properties of single components.

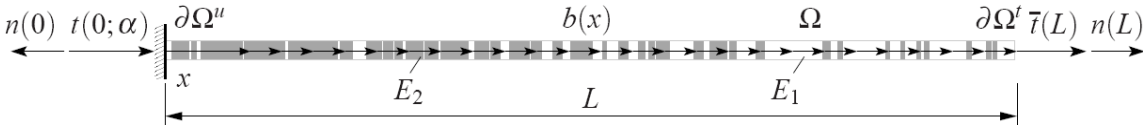

Fig. 3: One-dimensional elasticity problem associated with realization α

3.1. Problem statement

Consider a bar of unit cross-section area, represented by the interval $\Omega = (0,\, L)$ with the boundary $\partial\Omega = \{\, 0,\, L \,\}$, fixed at $\partial\Omega^u$, subject to a body force $b(x)$ and tractions $\bar{t}$ at $\partial\Omega^t$, see Figure 3. For a given realization α, the displacement field $u(x;\alpha)$ follows from the energy minimization problem

$$u(x;\alpha) = \arg\min_{v(x)\in\,\mathbb{V}}\ \Pi(\,v(x);\alpha), \tag{4}$$

where $\mathbb{V}$ denotes the *realization-independent* set of kinematically admissible displacements, v is a test displacement field and the energy functional Π is defined as:

$$\Pi(u(x);\alpha) = \frac{1}{2}\int_\Omega \varepsilon\big(v(x)\big) E(x;\alpha)\varepsilon\big(v(x)\big)\,\mathrm{d}x - \int_\Omega v(x)b(x)\mathrm{d}x - \big(v(x)\bar{t}(x)\big)\Big|_{\partial\Omega^t} \tag{5}$$

with the strain field $\varepsilon\big(v(x)\big) = \dfrac{dv}{dx}x$ and the Young modulus E in the form

$$E(x;\alpha) = \chi_1(x;\alpha)E_1 + \chi_2(x;\alpha)E_2, \tag{6}$$

where E_i denotes the *deterministic* Young modulus of the i-th phase.

In order to examine the distribution of minimizers for a given probability distribution $p(\alpha)$, we introduce the averaged energy functional Luciano (2005)

$$\Pi(\,v(x,\alpha)) = \int_{\mathbb{S}} (\,v(x;\alpha);\alpha)\,p(\alpha)d\alpha \tag{7}$$

and solve the associated variational problem

$$u(x,\alpha) = \arg\min_{v(x,\,\alpha)\in\,\mathbb{V}\times\mathbb{S}}\ \Pi(v(x;\alpha)). \tag{8}$$

In theory, the previous relation fully specifies the distribution of displacement fields. The exact specification of the set $\mathbb{S}$ is, however, very complex and the probability distribution $p(\alpha)$ is generally not known. Therefore, the solution needs to be based on partial geometrical data such as the one- and two-point probability functions introduced in section 2.

3.2. Hashin-Shtrikman decomposition

Following the seminal ideas of Hashin and Shtrikman, (1962) and Willis, (1977) the solution of the stochastic problem is sought as a superposition of two auxiliary problems, each characterized by constant material data E^0

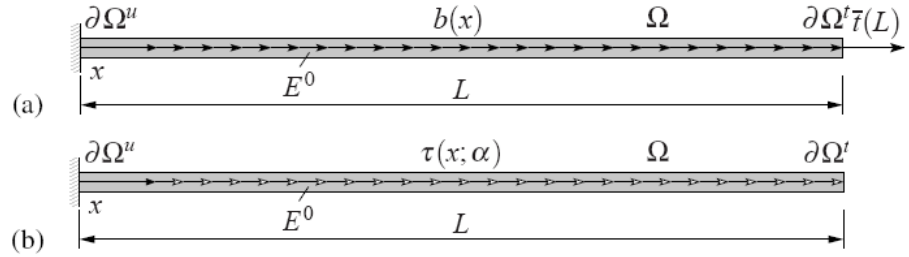

Fig 4. :. Problem decomposition; (a) deterministic reference case, (b) stochastic polarization problem.

In the first "reference" case, see Figure 4(a), the homogeneous structure is subject to the body force b and the boundary tractions $\bar{t}$ .The second "polarization problem", shown in Figure 4(b), corresponds to a homogeneous body loaded by polarization stress τ arising from the stress equivalence conditions:

$$\sigma(x;\alpha) = E(x;\alpha)\ \varepsilon(x;\alpha) = E^0\varepsilon(x;\alpha) + \tau(x;\alpha). \tag{9}$$

The unknown polarization stress now becomes a new variable to be determined from the critical point of the two-field Hashin-Shtrikman-Willis functional; e.g. Willis,(1977), Procházka and Šejnoha, (2004) and Bittnar and Šejnoha, (1996), Chapter 1.8.

$$\left(u(x;\alpha),\ \tau(x;\alpha)\right) = \arg \min_{v(x)\in\mathbb{V}} \ \operatorname{stat}_{\theta(x;\alpha)\in\mathbb{T}(\alpha)} U(v(x),\theta(x;\alpha);\alpha) \tag{10}$$

where θ denotes an admissible polarization stress from the *realization-dependent* set $\mathbb{T}(\alpha)$ and a new energy functional U is defined as

$$\begin{aligned} U(v(x),\theta(x;\alpha);\alpha) = \frac{1}{2}\int_\Omega \varepsilon\left(v(x)\right)E^0(x;\alpha)\varepsilon\left(v(x)\right)\mathrm{d}x - \int_\Omega v(x)\ b(x)dx - \left(v(x)\bar{t}(x)\right)\Big|_{\partial\Omega^t} + \\ + \int_\Omega \theta(x;\alpha)\varepsilon\left(v(x)\right)dx + \frac{1}{2}\int_\Omega \theta(x;\alpha)\left(E(x;\alpha) - E^0\right)^{-1}\theta(x;\alpha)dx. \end{aligned} \tag{11}$$

The minimization with respect to v in equation (10) can be efficiently performed using Green's function technique. To that end, we introduce a decomposition of the displacement field

$$u(x;\alpha) = u^0(x) + u^1(x;\alpha), \tag{12}$$

where u^0 solves the reference problem while u^1 denotes the displacement field related to the loading by a test stress polarization field θ. Note that the determination of u^0 is a standard task, which can be generally solved by a suitable numerical technique (cf. section 4.1 and section 4.2). By introducing the Green function of the reference problem satisfying

$$E^0\frac{\partial^2 G}{\partial x^2}(x,y) + \delta(x-y) = 0 \tag{13}$$

with boundary conditions (n denotes the outer normal, recall Fig. 4)

$$G(x,y) = 0 \text{ for } x\in\ \partial\Omega^u, \qquad T^0(x,y) = E^0\frac{\partial G(x,y)}{\partial x}n(x) = 0 \text{ for } x\in\ \partial\Omega^t, \tag{14}$$

we relate the u^1 component and the associated strain field ε^1 to the polarization stresses θ via, cf. (Luciano and Willis, 2005),

$$\begin{aligned} u^1(x;\alpha) &= -\int_\Omega \frac{\partial G^0(x,y)}{\partial y}\theta(y;\alpha)dy = -\int_\Omega \Gamma^0(x,y)\theta(y;\alpha)\mathrm{d}y, \\ \varepsilon\left(u^1(x;\alpha)\right) &= -\int_\Omega \frac{\partial^2 G(x,y)}{\partial x\partial y}\theta(y;\alpha)\mathrm{d}y = -\int_\Omega \Delta^0(x,y)\theta(y;\alpha)\mathrm{d}y. \end{aligned} \tag{15}$$

By exploiting the optimality properties of the minimizing displacement $u(x;\alpha)$ and upon exchanging the order of optimization, Equation (11) can be, after some steps described in, e.g. Willis, (1981), Luciano and Willis, (2005), recast solely in terms of the polarizations:

$$\tau(x;\alpha) = \arg \underset{\theta(x;\alpha)\in\mathbb{T}(\alpha)}{\text{stat}} H\left(\theta(x;\alpha);\alpha\right) \tag{16}$$

where the ``condensed'' energy functional is defined as

$$\begin{aligned} H\left(\theta(x;\alpha);\alpha\right) = \min_{v(x)\in\mathbb{V}} U(v(x),\left(x;\alpha\right);\alpha) = \Pi^0(u^0(x)) + \int_\Omega (x;\alpha)\varepsilon\left(u^0(x)\right)\mathrm{d}x \\ -\frac{1}{2}\int \theta(x;\alpha)\left(E(x;\alpha) - E^0\right)^{-1}\theta(x;\alpha)\mathrm{d}x \\ -\frac{1}{2}\int_\Omega\int_\Omega \theta(x;\alpha)\Gamma^0(x,y)\theta(y;\alpha)n\mathrm{d}x\mathrm{d}y \end{aligned} \tag{17}$$

with Π^0 denoting the total energy of the reference structure.

With the Hashin-Shtrikman machinery at hand, the stochastic problem introduced by Equation (7) can be solved by repeating the previous arguments in the probabilistic framework. In particular, taking the ensemble average of (12) and (15) yields

$$\langle u\rangle(x) = u^0(x) - \int_\Omega \Delta^0(x,y)\ \langle\tau\rangle(y)\mathrm{d}y \tag{18}$$

where the expectation $\langle\tau\rangle$ is a solution of the variational problem

$$\langle\tau\rangle(x) = \arg \underset{\theta(x;\alpha)\in\mathbb{T}(\alpha)\times\mathbb{S}}{\text{stat}} \mathsf{H}\left(\theta(x;\alpha);\alpha\right) \ \text{ with } \ \mathsf{H}\left(\theta(x;\alpha);\alpha\right) = \int_{\mathbb{S}}\left(\theta(x;\alpha);\alpha\right)p(\alpha)\mathrm{d}\alpha. \tag{19}$$

Due to limited knowledge of detailed statistical characterization of phase distribution, however, the previous variational problem can only be solved approximately. In particular, we postulate the following form of polarization stresses:

$$\tau(x;\alpha) \approx \chi_1(x;\alpha)\tau_1(x) + \chi_2(x;\alpha)\tau_2(x), \quad \theta(x;\alpha) = \chi_1(x;\alpha)\theta_1(x) + \chi_2(x;\alpha)\theta_2(x), \tag{20}$$

where $\theta_r(x)$ are *realization-dependent* trial fields related to phase *r*. Plugging the approximation into equation(19) leads, after some manipulations detailed in e.g Willis, (1981), Sejnoha, (2000), to the variational principle

$$\begin{aligned} \left(\tau_1(x),\tau_2(x)\right) = \arg \underset{(\theta_1(x),\theta_2(x))}{\text{stat}} \Pi^0(u^0(x)) + \sum_{r=1}^{2}\int_\Omega S_r(x)\theta_r(x)\varepsilon\left(u^0(x)\right)\mathrm{d}x \\ -\frac{1}{2}\sum_{r=1}^{2}\int_\Omega S_r(x)\theta_r(x)\left(E_r - E^0\right)^{-1}\theta_r(x)\mathrm{d}x \\ -\frac{1}{2}\sum_{r=1}^{2}\sum_{s=1}^{2}\int_\Omega\int_\Omega \theta_r(x)S_{rs}(x,y)\Gamma^0(x,y)\theta_s(y)\mathrm{d}x\mathrm{d}y; \end{aligned} \tag{21}$$

i.e. the "true" phase polarization stresses τ_r satisfy the optimality conditions (r=1,2)

$$\int_\Omega S_r(x)\left(E_r - E^0\right)^{-1}\tau_r(x)\mathrm{d}x + \sum_{s=1}^{2}\int_\Omega\int_\Omega S_{rs}(x,y)\Gamma^0(x,y)\tau_s(y)\mathrm{d}y\mathrm{d}x = \int_\Omega S_r(x)\varepsilon\left(u^0(x)\right)\mathrm{d}x \tag{22}$$

3.3. Discretization

The conditions (22) still present an infinite system to be fulfilled. Two ingredients are generally needed to convert them to the finite-dimensional system: (i) representation of the reference strain field and the Green function-related quantities and (ii) discretization of the phase polarization stresses. The first step is dealt with in detail in Section 4, now it suffices to consider the approximations $\varepsilon^{0,h_0}, \Delta^{0,h_0}$ and Γ^{0,h_0}.

where h_0 denotes a parameter related to the discretization of the reference problem.

Next, we reduce Eq.(22) to a finite-dimensional format using the standard Galerkin procedure. To that end, we introduce the following discretization of the phase polarization stresses

$$\tau_r(x) \approx \mathbf{N}^{\tau h_1} \boldsymbol{d}_r^{\tau h_0 h_1}, \quad \theta_r(x) \approx \mathbf{N}^{\tau h_1} \boldsymbol{d}_r^{\theta h_1}, \tag{23}$$

where $\mathbf{N}^{\tau h_1}$ is the matrix of (possibly discontinuous) shape functions controlled by the discretization parameter h_1; $\boldsymbol{d}_r^{\theta h_1}$ and $\boldsymbol{d}_r^{\tau h_0 h_1}$ denote the degrees-of-freedom (DOFs) of trial and true polarization stresses, the latter related to the discrete Green function. Introducing the approximations (23) into the variational statement (22) and using the arbitrariness of $\boldsymbol{d}_r^{\theta h_1}$ leads to a system of linear equations

$$\mathbf{K}_r^{\tau h_1} \boldsymbol{d}_r^{\tau h_0 h_1} + \sum_{s=1}^{2} \mathbf{K}_{rs}^{\tau h_0 h_1} \boldsymbol{d}_s^{\tau h_0 h_1} = \mathbf{R}_r^{\tau h_0 h_1} \tag{24}$$

with the individual terms given by (r,s=1,2)

$$\begin{aligned}
\mathbf{K}_r^{\tau h_1} &= \int_\Omega S_r(x) \mathbf{N}^{\tau h_1}(x)^T \left[E_r - E^0 \right]^{-1} \mathbf{N}^{\tau h_1}(x)\, dx, \\
\mathbf{K}_{rs}^{\tau h_0 h_1} &= \int_\Omega \int_\Omega S_{rs}(x,y) \mathbf{N}^{\tau h_1}(x)^T \Gamma^{0,h_0}(x,y) \mathbf{N}^{\tau h_1}(y)\, dx dy, \\
\mathbf{R}_r^{\tau h_0 h_1} &= \int_\Omega S_r(x) \mathbf{N}^{\tau h_1}(x)^T \boldsymbol{\varepsilon}^{0,h_0}(x)\, dx
\end{aligned} \tag{25}$$

Finally, once the approximate values of phase polarization stresses are available, the elementary statistics of the displacement field follow from the discretized form of Eq.(18)

$$\langle u \rangle(x) = \langle u \rangle^{h_0 h_1}(x) = u^{0,h_0}(x) - \sum_{r=1}^{2} \left(\int_\Omega \Delta^{0,h_0}(x,y) S_r(y) \mathbf{N}^{\tau h_1}(y)\, dy \right) \boldsymbol{d}_r^{\tau h_0 h_1}. \tag{26}$$

Note that additional information such as conditional statistics or higher-order moments can be extracted from the polarization fields in post-processing steps similar to Eq.(26); see Luciano and Willis, (2005, 2006), Lombardo et al., (2008) for more details.

4. Solution of reference problem

4.1. Finite element method

The solution of the reference problem follows the standard Finite Element procedures. Nevertheless, we briefly repeat the basic steps of the method for the sake of clarity. The reference displacement u^0 follows from the identity

$$\int_\Omega \boldsymbol{\varepsilon}(v(x)) E^0 \boldsymbol{\varepsilon}(u^0(x))\, dx = \int_\Omega v(x) b(x) dx + \left(v(x) \bar{t}(x) \right)\Big|_{\partial\Omega^t} \tag{27}$$

which should hold for any test function $v \in \mathbb{V}$. Within the conforming finite element approach, the unknown displacement u^0 and the test function v together with the associated strain field are sought in a finite-dimensional subspace $\mathbb{V}^{h_0} \subset \mathbb{V}$

$$u^0(x) \approx u^{0,h_0}(x) = \mathbf{N}^{uh_0}(x) \boldsymbol{d}^{uh_0}, \quad v^0(x) \approx v^{h_0}(x) = \mathbf{N}^{uh_0}(x) \boldsymbol{d}^{vh_0}, \tag{28}$$

$$\boldsymbol{\varepsilon}(u^0(x)) \approx \boldsymbol{\varepsilon}(u^{0,h_0}(x)) = \mathbf{B}^{uh_0}(x) \boldsymbol{d}^{uh_0}, \quad \boldsymbol{\varepsilon}(v(x)) \approx \boldsymbol{\varepsilon}(v^{h_0}(x)) = \mathrm{B}^{uh_0}(x) \boldsymbol{d}^{vh_0}, \tag{29}$$

where $\mathbf{N}^{\mathrm{uh}}{}_0$ is the displacement interpolation matrix and $\mathbf{B}^{\mathrm{uh}}{}_0$ denotes the displacement-to-strain matrix. Using the discretized fields Eq.(27), reduces to the system

$$\mathbf{K}^{uh_0}\boldsymbol{d}^{uh_0} = \mathbf{R}^{uh_0} \tag{30}$$

Solving the system for $\boldsymbol{d}^{uh_0}$ enables us to obtain the ε^{0,h_0} approximation using Eq. (29).

The discretized version of the Green function follows from Eq. (27) with $\bar{t} = 0$ and $b = \delta(y - x)$.

$$G^0(x,y) \approx G^{0,h_0}(x,y) = \mathbf{N}^{uh_0}(x)\left(\mathbf{K}^{uh_0}\right)^{-1}\mathbf{N}^{uh_0}(y)^T \tag{31}$$

The remaining Green function-related quantities can now be expressed directly from Eq. (15) leading to

$$\Delta^0(x,y) \approx \Delta^{0,h_0}(x,y) = \mathbf{N}^{uh_0}(x)\left(\mathbf{K}^{uh_0}\right)^{-1}\mathbf{B}^{uh_0}(y)^T \tag{32}$$

$$\Gamma^0(x,y) \approx \Gamma^{0,h_0}(x,y) = \mathbf{B}^{uh_0}(x)\left(\mathbf{K}^{uh_0}\right)^{-1}\mathbf{B}^{uh_0}(y)^T. \tag{33}$$

4.2. Boundary element discretization.

Following the standard Boundary Element Method procedures, we start from the Betti identity written for the reference problem:

$$\int_\Omega \frac{\partial^2 v}{\partial \xi^2}(\xi)\,E^0 u^0(\xi)\,d\xi = \left(n(\xi)\varepsilon\left(v(\xi)\right)E^0 u^0(\xi) - v(\xi)t^0(\xi)\right)\Big|_{\partial\Omega(\xi)} - \int_\Omega v(\xi)b(\xi)d\xi \tag{34}$$

and apply the test displacement in the form

$$v(\xi) = G^{0,\infty}(\xi, x) \tag{35}$$

where $G^{0,\infty}$ is the infinite body Green's function.

The integral identity (34), written for any $x \in \Omega$, receives the form, (Sharif Khodaei, 2006, Section 6.2)

$$u^{0,h_0}(x) = \left(G^{0,\infty}(x,\xi)t^{0,h_0}(\xi) - T^{0,\infty}(x,\xi)u^{0,h_0}(\xi)\right)\Big|_{\partial\Omega(\xi)} + \int_\Omega G^{0,\infty}(x,\xi)b(\xi)\,d\xi \tag{36}$$

The associated strain field can be expressed as:

$$\varepsilon^{0,h_0}(x) = \left(\frac{\partial G^{0,\infty}(x,\xi)}{\partial x}t^{0,h_0}(\xi)\right)\Big|_{\partial\Omega(\xi)} + \int_\Omega \frac{\partial G^{0,\infty}(x,\xi)}{\partial x}b(\xi)d\xi \tag{37}$$

Analogously to the Finite Element treatment, the expression for the finite-body Green function starts from Eq.(34) with $b = \delta(y - \xi)$ and boundary data (14). Following the specific form of Eq. (36) (and allowing for a slight inconsistency in notation), we introduce a decomposition of the Green function into the discretization-independent infinite-body part and the discretization-dependent boundary contribution:

$$G^0(x,y) \approx G^{0,\infty}(x,y) + G^{0,h_0}(x,y). \tag{38}$$

Expressions for Δ^0 and Γ^0 are derived following an analogous procedure. We exploit the infinite-body-boundary split:

$$\Delta^0(x,y) \approx \Delta^{0,\infty}(x,y) + \Delta^{0,h_0}(x,y) \tag{39}$$

$$\Gamma^0(x,y) \approx \Gamma^{0,\infty}(x,y) + \Gamma^{0,h_0}(x,y) \tag{40}$$

Finally note that the previous procedure can be directly translated to multi-dimensional and/or vectorial case; see Procházka and Šejnoha, (2003), (Section 3) for more details.

5. Numerical examples

For the numerical example studied in this work the following basis functions and integration schemes are employed, based on a uniform partitioning of Ω into N_e cells Ω_e of length $h_1 = L / N_e$ are defined by Figure 5.In particular, the specification of the polarization stress in terms of $\mathbb{P}_0$ shape functions requires $2N_e$ DOFs, while $\mathbb{P}_1$ and $\mathbb{P}_{-1}$ discretizations are parametrized using $2(N_e+1)$ or $4N_e$ values respectively.

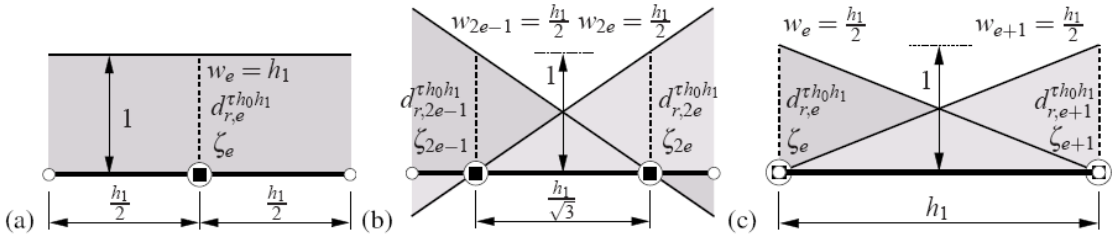

Fig 5: Choice of shape functions and integration points related to *e*-th cell; (a)piecewise-constant basis functions $\mathbb{P}_0$ and the Gauss-Legendre quadrature of order 1 (GL_1), (b) piecewise-linear discontinuous basis functions $\mathbb{P}_{-1}$ and the Gauss-Legendre quadrature of order 2 (GL_2), (c)piecewise linear continuous basis functions $\mathbb{P}_1$ and Newton-Cotes quadrature of order 1(NC_1);○ cell nodes, ○ degrees of freedom, ■ integration points

The following factors have a significant influence on the accuracy of the discrete Hashin-Shtrikman scheme:

- approximation of the Green function of the comparison body,
- basis functions and numerical quadrature used to discretize the polarization problem,
- Young's modulus of the reference body E^0
- contrast of the Young moduli of individual phases (E_2 / E_1)
- characteristic size of microstructure with respect to the analyzed domain (l / L)

All these aspects are studied in details in the rest of this Section. Two representative examples of structures subject to a uniform body force *b* and homogeneous mixed and boundary data are considered, see Figure 6. The heterogeneity distribution is quantified according to the model introduced in Section 2. Moreover, we systematically compare the obtained numerical results against reliable reference values determined by extensive Monte-Carlo (MC) simulations.

5.1. Direct simulation results

For the purpose of the following discussion, the reference values of the average displacement fields $\langle u \rangle_{MC}(x)$ together with the 99.9% interval estimates $\left[\langle u_- \rangle_{MC}(x), \langle u_+ \rangle_{MC}(x)\right]$ are understood as the piecewise linear interpolants of discrete data sampled by MC procedure. In addition, the homogenized displacement $u_H(x)$ field is introduced to assess the performance of the local averaging approach. Figure 6 shows several representative results plotted using dimensionless quantities.

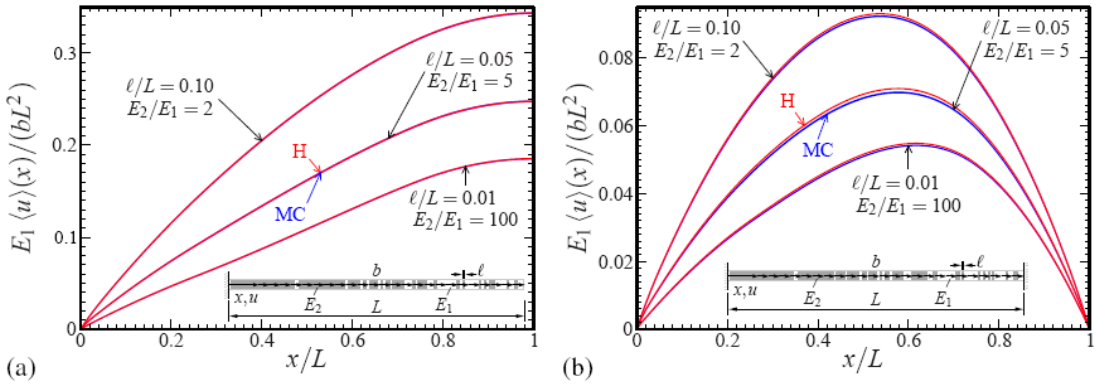

Fig 6: Reference Monte-Carlo solution; (a) statically determinate and (b) indeterminate problems; MC results correspond to 99.9% confidence interval estimates, H refers to homogenized solution.

As apparent from Figure 6, the obtained statistics of overall response exhibits rather narrow confidence intervals, implying the reliability and accuracy of the MC estimates. For the statically determinate structure, the locally homogenized solution coincides with the ensemble average of the displacement fields, as demonstrated by the overlap of simulation results with homogenized data. The converse is true (with the 99.9% confidence) for the statically indeterminate case, where these two results can be visually distinguished from each other. The mismatch (which increases with increasing (E_2 / E_1) and decreasing (l / L) provides an elementary demonstration of the fact that even in the one-dimensional setting the local averaging may lead to incorrect values when treating non-homogeneous random media. Such effect does not appear in the deterministic setting, where the harmonic average is known to represent the homogenized solution exactly, cf. Murat and Tartar (1997). This result naturally justifies the application of approaches based on higher-order statistics, with the H-S method being the most prominent example.

5.2. Effect of the Green function approximation

In order to illustrate the effect of approximate Green's function, we restrict our attention to the statistically determinate structure and employ the standard piecewise linear basis functions N^{uh_0} to evaluate Γ^{uh_0} function in the FEM setting using Equation(33). Figure 7 allows us to perform the qualitative assessment of the results for different choices of basis functions, the integration scheme and the discretization parameter h_0.

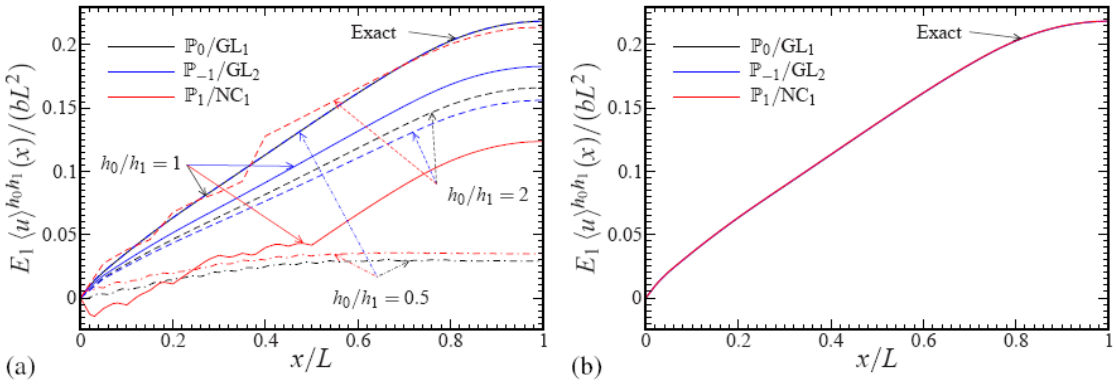

Fig 7: Influence of approximate Green's function for the statically determinate problem; (a) FEM-based solution, (b) BEM-based solution $E_2 / E_1 = 10$, $E^0 / E_1 = 5$, $l / L = 0.1$, $h_1 / L = 0.25$.

Evidently, a suitable choice of discretization parameter h_0 is far from being straightforward. From all the possibilities presented in Figure 7(a), only the combinations $h_1 = h_0$ with $\mathbb{P}_0 / \mathrm{GL}_1$ discretization of the polarization problem and $h_1 = 2h_0$ with $\mathbb{P}_{-1} / \mathrm{GL}_2$ scheme are capable of reproducing the homogenized solution, while all the remaining possibilities lead to inaccurate results often accompanied by an oscillatory response. On the other hand, the BEM-based solution shows correct response for all reported discretization of the polarization problem. Moreover, the results confirm good performance of $\mathbb{P}_0$ and $\mathbb{P}_1$ schemes when compared to the $\mathbb{P}_{-1}$ discretization, which requires about twice the number of DOFs of former schemes for the same cell dimensions h_1 (recall Figure 5). Similar conclusions can also be drawn for the statically indeterminate case. Therefore, we concentrate on the BEM approach in the sequel and limit the choice of basis functions to $\mathbb{P}_0$ and $\mathbb{P}_1$ only.

5.3. Influence of the integration scheme and basis functions

Thus far, we have investigated the combination of numerical quadratures and shape functions, for which the location of integration points coincides with the position of DOFs. Figure 8 shows the convergence plots for the relevant basis function/integration scheme pairs. To address also the statically determinate case, the relative error is now related to MC data, leading to the definition

$$\eta_{MC}^{h_0 h_1} = \frac{\left\| \langle u \rangle^{h_0 h_1}(x) - \langle u \rangle_{MC}(x) \right\|_{L_2(\Omega)}}{\left\| \langle u \rangle_{MC}(x) \right\|_{L_2(\Omega)}} \tag{41}$$

In addition, two comparative values are introduced: the relative error of the homogenized solution H and the relative error associated with $\langle u_- \rangle_{MC}$ or $\langle u_+ \rangle_{MC}$ function, appearing as the Interval Estimate (IE) line.

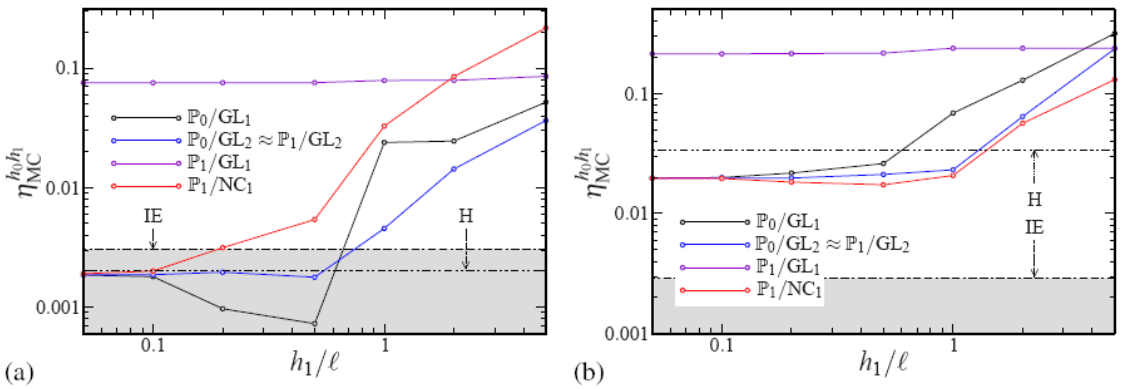

Fig 8.: Influence of the choice of numerical discretization; (a) statically determinate and (b) indeterminate structures $E_2 / E_1 = 5$, $E^0 / E_1 = 3$, $l / L = 0.1$; IE denotes the error associated with the 99.9% confidence interval estimate.

For the determinate structure, the observed behavior is rather similar to the one reported in Section 5.2. In particular, Figure 8(a) confirms that the homogenized solution quickly reaches the accuracy comparable with the confidence intervals (indicated by the grey area) and eventually converges to the homogenized solution, with the exception of $\mathbb{P}_1/\mathrm{GL}_1$ combination resulting in a singular system matrix(24). Moreover, the superiority of the GL_2 quadrature over lower-order scheme is evident; the proper representation of spatial statistics seems to be more important than smoothness of the polarization shape functions.

Figure 8 (b) shows the results for the statically indeterminate case. With 99.9% confidence, the results *quantitatively* demonstrate that the homogenized solution differs from the MC data. The H-S solution, corresponding to an estimate pertinent to for the fixed value of parameter E^0 and *all* random 1D media characterized by the two-point statistics, gives the error about 50% of the value of the homogenized solution, but ceases to attain the accuracy set by the confidence interval.

5.4. Influence of the reference media and phase contrast

Having identified the intrinsic limitation of the H-S approach, we proceed with the last free parameter of the method: the choice of the reference medium. To that end, we introduce the following parametrization of the Young modulus

$$E^0 = (1-\omega) E_1 + \omega E_2. \tag{42}$$

Note that for the phases indexed such that $E_1 < E_2$, $\omega = 0$ and $\omega = 1$ correspond to the rigorous lower and upper bounds on the ensemble average of the energy and, consequently, to the positive- or negative-definite system matrix (Procházka and Šejnoha, 2004),(Luciano and Willis, 2005). The intermediate values lead to variational energetic estimates and to a symmetric system matrix. Figure 9 illuminates the effect of ω, plotted for three representative contrasts of phase moduli and h_1 / l ratios.

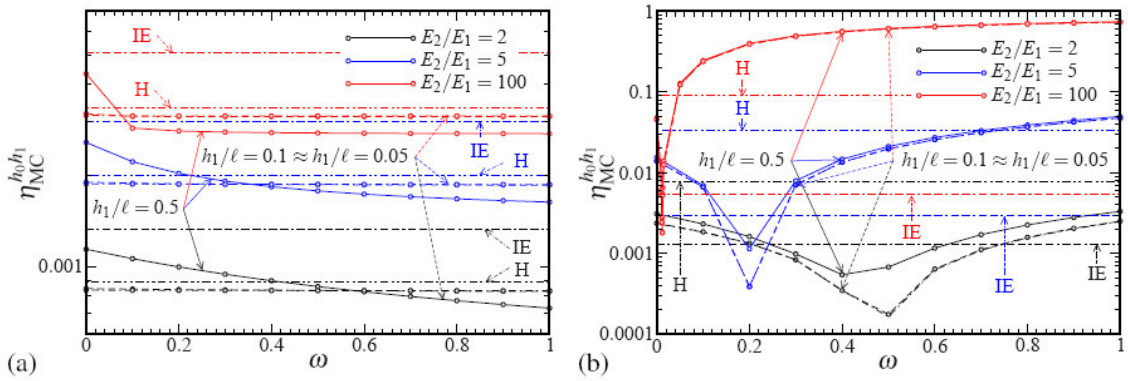

Fig. 9.: Influence of the choice of the reference media; (a) statically determinate and (b) indeterminate structures; $l / L = 0.1$, $\mathbb{P}_0 / \mathrm{GL}_2$ discretization.

In the first case, see Figure 9 (a), the choice of the reference media has almost negligible effect on the H-S solution error; the slight influence observed for the coarse discretization completely disappears upon cell refinement. This is not very surprising as the homogenized solution depends on the first-order statistics only, and as such can be retained by the discrete H-S method (up to controllable errors) for any choice of E^0. Results for the statically indeterminate structure, on the other hand, show a significant sensitivity to the value of ω. By a proper adjustment of the reference medium, the error can be reduced by an order of magnitude and eventually reach the accuracy of extensive MC sampling. With increasing phase moduli contrast, however, the range of such ω values rapidly decreases; e.g. for $E_2 / E_1 = 100$ one needs to satisfy $9.10^{-4} \lesssim \omega \lesssim 1,5.10^{-3}$ in order to recover the MC results. It is noteworthy that these values agree rather well with the particular choice of reference media used by Matouš (2003), when modeling of composites with a high phase contrast using the methodology proposed by Dvorak and Srinivas(1999).

5.5. Influence of microstructure size

Eventually, we investigate the influence of the microstructure size. Figure 10 summarizes the obtained results for a moderate phase contrast and the optimal setting of the H-S method identified in the previous sections. A similar trend can be observed for the both case studies: for all three l / L values, the H-S method is capable of reaching the error associated with the MC confidence intervals for the cell length h_1 approximately equal to a half of the microscopic lengthscale l. In other words, keeping the same number of DOFs used to discretize the polarization problem, the accuracy of the method increases with the increasing l / L ratio, which is exactly the opposite trend than exhibited the one observed for the homogenized solution.

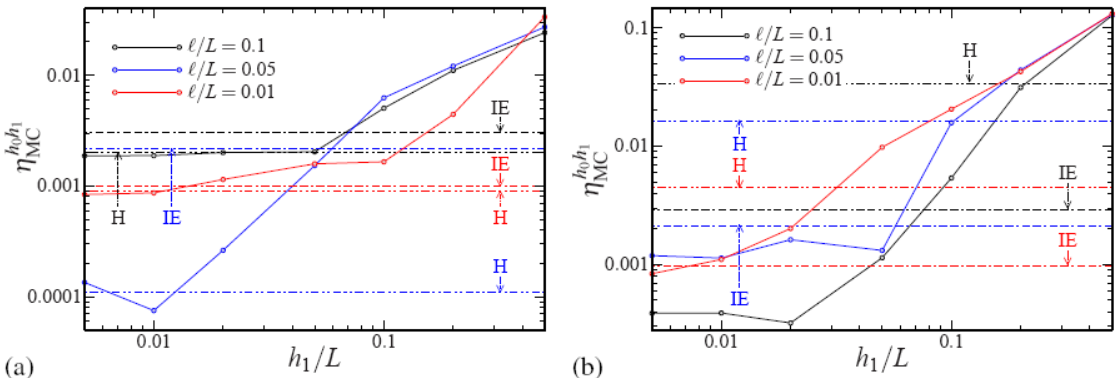

Fig 10.: Influence of microstructure size; (a) statically determinate and (b) indeterminate structures; $E_2 / E_1 = 5$, $\omega = 0.2$, $l / L = 0.05$, $\mathbb{P}_0 / \mathrm{GL}_2$ discretization.

6. Conclusions

In the present work, the predictive properties of numerical methods based on the Hashin-Shtrikman-Willis variational principles, when applied to specific model of functionally graded materials, have been systematically assessed. By restricting our attention to the one-dimensional setting, an extensive parametric study has been executed and the results of numerical schemes have been verified against reliable large-scale Monte-Carlo simulations. On the basis of obtained data, we conjecture that:

- The Hashin-Shtrikman based numerical method, when set up properly, is capable of delivering results with the accuracy comparable to detailed Monte Carlo simulations and, consequently, of outperforming the local averaging schemes.
- When applying the Finite Element method to the solution of reference problem, the employed discretization has to be compatible with the numerics used to solve the polarization problem. If this condition is satisfied, the additional FEM-induced errors quickly become irrelevant.
- For the discretization of the reference problem, it appears to be advantageous to combine low order (discontinuous) approximation of the polarization stresses with higher order quadrature scheme to concisely capture the heterogeneity distribution.
- The correct choice of the reference medium has the potential to substantially decrease the error. Unfortunately, apart from Dvorak and Srinivas (1999), we fail to give any a-priory estimates of the optimal value for statistically non-homogeneous structures.
- For accurate results, the characteristic cell size should be around 2-5 times smaller than the typical dimensions of the constituents.

The bottleneck of the current implementation is the solution of system(24), since it leads to a fully populated system matrix. Fortunately, as illustrated by Figure 11, the conditioning of the polarization problem seems to be mainly dominated by the phase contrast rather than the discretization of the reference problem, which opens the way to efficient iterative techniques. In addition, more qualitative understanding of the discrete Green function effect seems to be necessary.

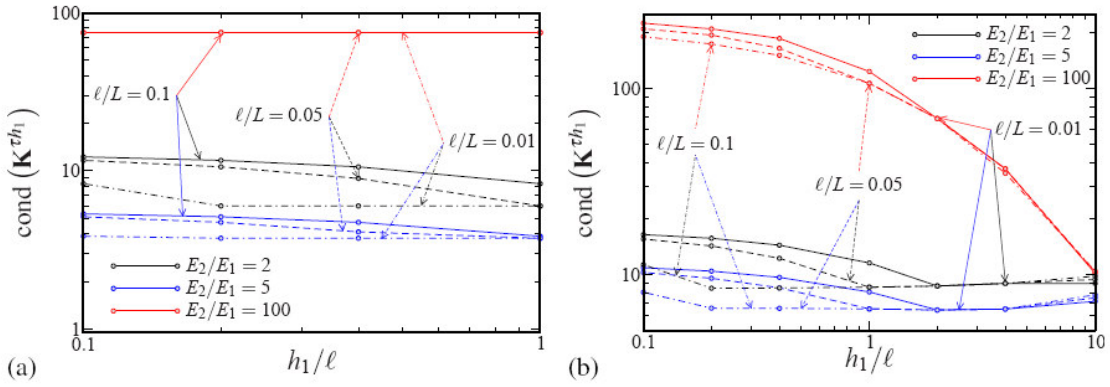

Fig.11.: Sensitivity of conditioning of system matrix of the polarization problem; (a) statically determinate and (b) indeterminate structures; $l/L=0.05$, $\omega=0.2$, $\mathbb{P}_0/\mathrm{GL}_2$ scheme, the condition number is estimated using Higham and Tisseur, (2000) algorithm.

The next extension of the method would involve treatment of the multi-dimensional setting. Specific non-linear and time-dependent material behavior can be treated using tools of continuum micromechanics, see e.g. Ponte Castañeda and Suquet, (1998), and eventually combined with optimization in the spirit of Molchanov et al., (2000). Such work will be reported separately in our future publications.

Acknowledgments

The first author acknowledges the support of this research from project No.103/07/0304 (GA ČR), the work of the second author was supported from the research project MSM 6840770003 (MŠMT ČR).

References

Bendsøe, M. and Sigmund, O. (2004). Topology optimization. Springer, second edition.

Beran, M. J. (1968). Statistical Continuum Theories. Monographs in Statistical Physics. Interscience Publishers.

Bittnar, Z. and Šejnoha, J. (1996). Numerical methods in structural mechanics. ASCE Press and Thomas Telford, Ltd, New York and London.

Böhm, H. (2005). A short introduction to basic aspects of continuum micromechanics. Technical Report hjb/ILSB 050103, Christian Doppler Laboratory for Functionally Oriented Materials Design, Institute of Lightweight Design and Structural Biomechanics, Vienna University of Technology.

Buryachenko, V. and Rammerstorfer, F. (2001). Local effective thermoelastic properties of graded random structure matrix composites. Archive of Applied Mechanics, 71(4–5):249 272.

Buryachenko, V. A. (2001). Multiparticle effective field and related methods in micromechanics of composite materials. Applied Mechanics Reviews, 54(1):1–47.

Cho, J. R. and Ha, D. Y. (2001). Averaging and finite-element discretization approaches in the numerical analysis of functionally graded materials. Materials Science and Engineering A, 302(2):187–196.